ON THE THERMODYNAMIC CYCLE OF A MEMS-BASED EXTERNAL COMBUSTION RESONANT ENGINE

H. Bardaweel[1], R. Richards[1*], C. Richards[1], & M. Anderson[2]

[1] School of Mechanical and Materials Engineering, Washington State University, Pullman, USA
[2] Dept. of Mechanical Engineering, University of Idaho, Moscow, USA
*Presenting Author: heatran@wsu.edu

Abstract: In this work we investigate the thermodynamic cycle of a resonant, MEMS-based, micro heat engine. The micro heat engine is made of a cavity encapsulated between two membranes. The cavity is filled with saturated liquid-vapor mixture working fluid. Heat is added/rejected from the engine at a frequency equal to its resonant frequency. Both pressure-volume and temperature-entropy diagrams of the resonant engine are used to investigate the thermodynamic cycle of the resonant micro heat engine. The measured second law efficiency of the micro heat engine is 16%.

Keywords: micro heat engine, MEMS engine, resonant heat engine

INTRODUCTION

Development of micro-scale heat engines based on the Rankine cycle [1], Otto cycle [2], Brayton cycle [3], Stirling cycle [4], and Humphrey cycle [5] has been proposed by different research groups. Our group has developed a resonant micro-scale dynamic heat engine that is not based on these standard cycles. The resonant micro heat engine is an external combustion engine with a design based on stacking 2D structures. In previous work we have characterized the performance of the engine off-resonance and demonstrated power production [6]. The resonant frequency of the engine was determined to be on the order of 100 Hz [7].

In this work we look at the thermodynamic cycle of this resonant micro heat engine. In previous work we have shown that resonant operation of the micro heat engine is beneficial [7]. That is, for a resonant operation pressure and volume in the engine cavity are decoupled, i.e. cyclically rise and fall 90 degrees out of phase [7]. To characterize the cycle of the resonant engine both pressure and volume inside the engine cavity are measured. Assuming saturation conditions and using pressure measurements both temperature and entropy inside the engine cavity are estimated. Pressure-volume and temperature-entropy diagrams are then used to characterize the thermodynamic cycle of the resonant engine.

EXPERIMENT

Figure 1 shows a schematic of the resonant micro heat engine. The cavity of the engine is filled with a two-phase mixture of 3M™ PF5060DL fluid. The cavity is encapsulated between two thin membranes. The top membrane acts as an expander/compressor. The bottom membrane acts as an evaporator. A capillary wick fabricated on top of the evaporator membrane controls the thickness of the liquid-phase layer inside the cavity. A small mass is placed on top of the expander membrane. The purpose of the added mass is to reduce the resonant frequency of the engine to the order of 100Hz. Lastly, a thermal switch is used to control the timing and duration of the heat addition and heat rejection processes. Details on fabrication of engine components are provided in [6-8].

Figure 2 illustrates the experimental apparatus used to characterize the thermodynamic cycle of the engine. The engine is mounted on top of a sealed chamber. The chamber is filled with low thermal conductivity gas. The thermal switch consists of a liquid-metal micro-droplet array deposited on a silicon die. The die is bonded to a micro heat exchanger mounted on a piezo-stack actuator. A frequency generator delivers a sine wave voltage to control the stack actuator's displacement amplitude and frequency of operation. The motion of the piezo-stack actuator is transmitted to the micro heat exchanger through a push-pull device that seals against vacuum.

Heat is transferred to or from the engine when the micro-droplet array contacts the bottom evaporator membrane. In the experiments described in this paper, a thermal switch was used to control the heat rejection from the engine. However, a resistance heater was used for heat addition to the engine to enable precise control of the magnitude and duration of the heat

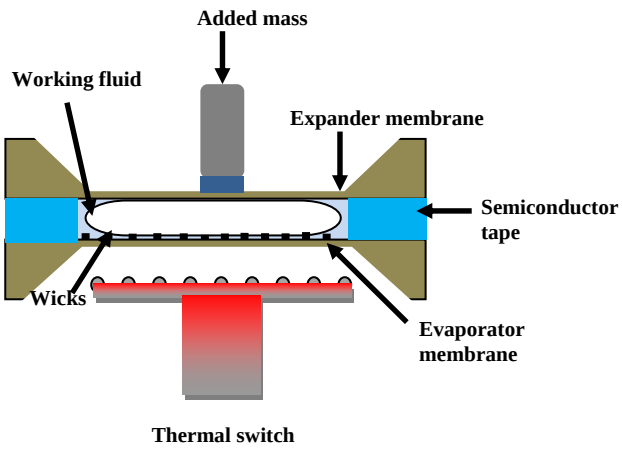

Fig.1. Schematic of micro heat engine.

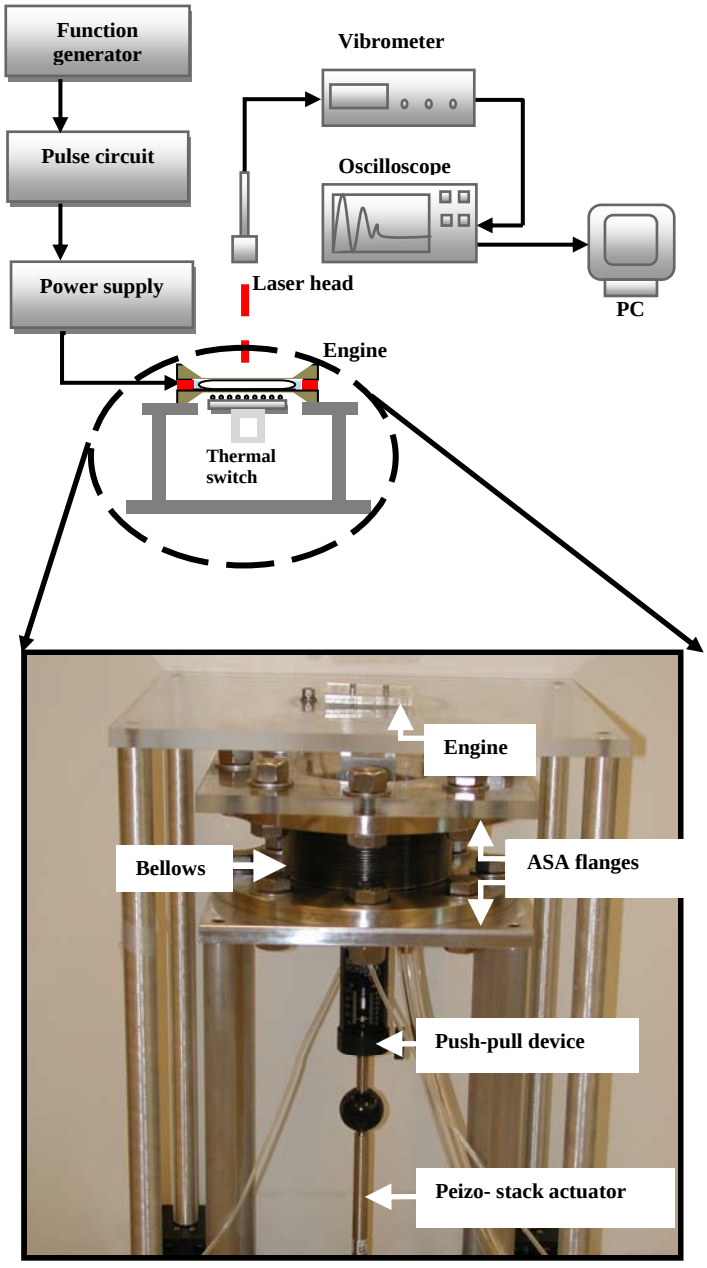

Fig. 2. Experimental setup apparatus.

addition process. The motion of the expander and evaporator membranes is measured with a laser vibrometer. The displacements of both expander and evaporator membranes are sampled with a digital oscilloscope and stored on a personal computer.

To characterize the thermodynamic cycle of the micro heat engine at resonance pressure P, volume V, temperature T, and entropy S inside engine cavity are determined. It is assumed that working fluid inside engine cavity is saturated and that the pressure and temperature inside the cavity are uniform. The pressure and volume measurements are decoupled during resonance operation. That is they are out of phase by 90 degrees. Because of this the pressure and volume changes are determined independently for a resonance operation. This is done by detecting the pressure and volume changes inside the engine using the deflection of the evaporator and expander membranes respectively. The volume underneath a membrane is determined by performing a double integral on the membrane deflection profile equation given by

$$\Delta V(\delta) = \frac{\delta}{a^4}\int_{-a}^{a}\int_{-a}^{a}(a^2-x^2)(a^2-y^2)\left[1+\frac{R}{a^2}(x^2+y^2)\right]dxdy \quad (1)$$

where δ is the deflection of the midpoint of the expander membrane in micrometer, a is ½ the side length of the membrane, x and y are coordinates on the membrane, and R=0.34 is a constant determined by matching the deflection profile of the equation to experimental data.

Pressure P is related to the deflection of the evaporator membrane through a calibrated pressure deflection curve of the form [9]

$$\Delta P = C_1\delta + C_2\delta^3 \quad (2)$$

where pressure P is in kPa, δ is the evaporator membrane deflection in micrometer. The constants C_1 and C_2 are determined by matching the deflection profile of the equation to experimental data. For the 2 μm thick, 64 mm^2 silicon evaporator membrane used in this work the constants C_1 and C_2 are $1.4197\ \text{X}10^{-2}$ and $8.4\,\text{X}10^{-6}$, respectively.

Based on pressure P and volume V measurements, the boundary work of the engine is defined as

$$W = \int PdV \quad (3)$$

The mechanical efficiency is then defined based on the boundary work W in (3) and the input energy delivered to the engine per cycle E, given by

$$\eta_{mech} = \frac{\int PdV}{E} \quad (4)$$

The Carnot efficiency is defined based on the maximum and minimum temperatures of the working fluid and given by

$$\eta_{Carnot} = 1 - \frac{T_{Li}}{T_{Hi}} \quad (5)$$

where T_{Li} and T_{Hi} are the minimum and maximum engine cavity temperatures, respectively. Using pressure measurements P, temperature inside the cavity T is interpolated from thermodynamic tables of 3M™ PF5060DL working fluid.

To specify the entropy S inside the cavity, two independent intensive properties are needed. Entropy S is obtained using quality and pressure information. The quality of the mixture $\overset{*}{Q}$ along with pressure P serve as the two intensive properties needed. The quality of the mixture $\overset{*}{Q}$ is calculated based on volume V and density ρ:

$$\overset{*}{Q} = \frac{V * \rho}{m_{total}} \tag{6}$$

The product $(V * \rho)$ represents the mass of vapor inside the cavity. The total mass of liquid-vapor mixture is given by m_{total}. The vapor density ρ is interpolated using thermodynamic tables of 3M™ PF5060DL working fluid. Entropy S is then given by

$$S = S_f + \overset{*}{Q} \bullet S_{fg} \tag{7}$$

$$S_{fg} = S_g - S_f \tag{8}$$

where S_g and S_f are entropies of saturated vapor and saturated liquid, respectively.

RESULTS AND DISCUSSION

Throughout this paper, the expander and evaporator are 300 nm thick silicon nitride and 2 μm thick silicon membranes, respectively. The side length of the expander membrane is 10 mm. The size of the saturated-vapor bubble is 9 mm. The thickness of the cavity is 150μm. The mass added to the engine is, m_{added}=3.9g. The wick structures are 5μm thick, 10μm high, and spaced 90μm apart. The resonant frequency of this particular engine is determined to be f_n=115 Hz. Details on measurement of resonant frequency are in [7]. In the experiment, the micro heat engine is operated at its resonant frequency, f_n=115Hz. Input energy per cycle, delivered to the evaporator, is E=1.0mJ and it is delivered with a 1% duty cycle. The thermal switch, controlling heat rejection, is maintained at 4°C during the operation of the engine. The experiment is carried out at room temperature, T_o=294K. The saturation pressure of the two-phase mixture inside the engine cavity is P_{sat}=25351Pa gage at room temperature T_o=294K.

Figure 3 shows the time history of pressure and volume inside the cavity when the engine is operated at resonance, f_n=115Hz. Volume and pressure inside engine cavity are obtained from (1) and (2), respectively. The figure shows that pressure and volume in the engine cavity are decoupled and cycle work is produced.

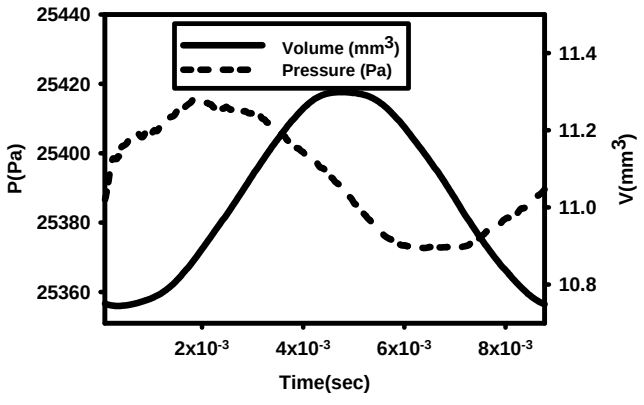

Fig. 3. Pressure and volume time history at resonance.

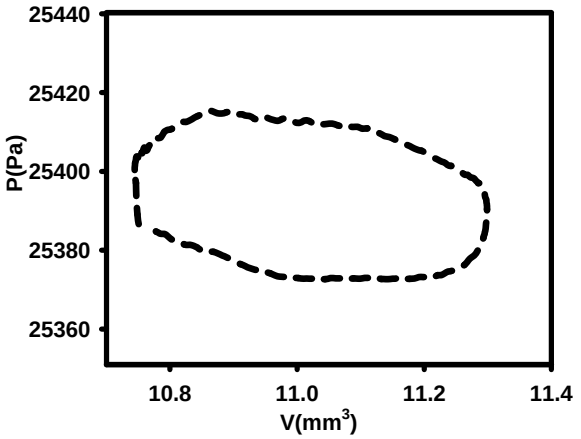

Fig. 4. Pressure-volume diagram.

The corresponding pressure-volume and temperature-entropy diagrams are shown in Figure 4 and 5, respectively. The cycle work is represented by the area enclosed by the pressure-volume and temperature-entropy diagrams. The maximum pressure rise and volume change inside the cavity are 45Pa and 0.55mm^3, respectively. The engine is operating over a very small temperature difference, on the order of 1K. At this condition the mechanical work produced by the micro engine in one cycle is 0.018μJ. The small operating temperature difference is due partly to the small amount of heat added and to the large thermal storage of the engine structure, the membranes and the wicks. That is, very little of the heat that is added to the engine goes to vaporizing working fluid, less than 10%.

To calculate the Carnot efficiency, the engine may be viewed as operating between the two temperature reservoirs at T_{Hi} and T_{Li} respectively. The second law efficiency, the ratio of the thermal efficiency to the Carnot efficiency is then found to be 16%. The thermal efficiency is evaluated from the ratio of the work produced by the working fluid to the energy added to the membrane.

From the pressure-volume and temperature-entropy diagrams it can be seen that the cycle is roughly rectangular in shape and consists of two constant temperature processes and two constant volume processes. Heat is transferred from the engine structure to vaporize the working fluid in a constant temperature process. During this process the membrane is moving outward and the vapor volume increases. After vaporization is completed, due to inertial effects, the membrane continues to move outwards for a short time and the temperature and pressure drop slightly. Once the expander membrane reaches its maximum deflection point, the thermal switch closes the gap with the evaporator membrane and heat is conducted away from the engine structure. Engine pressure and temperature decrease over a very small volume change. During resonant operation of

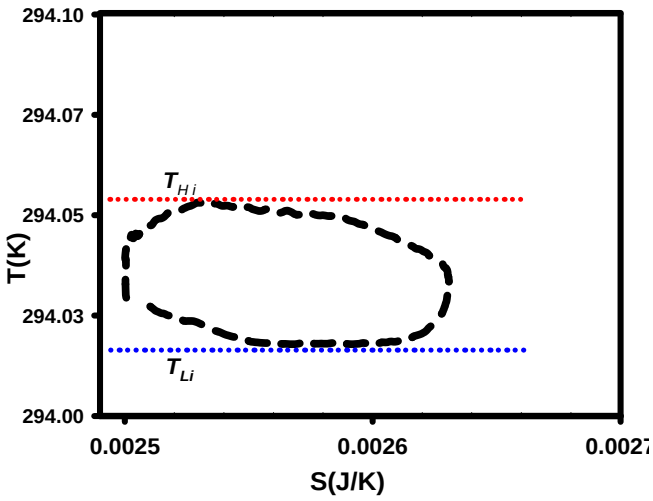

Fig. 5. Temperature entropy diagram.

the engine, potential energy is stored in the flexing expander membrane. This energy stored in the expander membrane now causes the membrane to flex in reducing the volume. During this process heat is removed from the vapor and condensation occurs at constant temperature. Again, due to inertial effects, the expander membrane continues to move down after condensation has ceased. When the membrane reaches its minimum deflection point, heat is added to the engine structure through the evaporator membrane. The inertial effects are relatively small in these experiments due to the small deflections resulting from small heat addition. With resonant operation at higher amplitudes, the inertial effects would become more dominant producing distinctive compression and expansion processes.

Engine irreversibility may be attributed to three major sources: (1) entropy production due to the finite temperature differences required to drive heat transfer during heat addition and rejection (2) entropy production due to heat transfer into and out of thermal storage in the engine, and (3) entropy production due to viscous losses in the liquid working fluid surrounding the vapor bubble. The first mechanism, entropy production due to heat transfer into and out of the engine, is a consequence of the fact that the engine is an external combustion device. The second mechanism, entropy production due to heat transfer into and out of thermal storage is a consequence of the resonant operation of the engine with its periodic heat addition and rejection processes. Finally, the third mechanism, entropy production due to viscous losses is a consequence of the motion of the liquid working fluid as the membrane flexes in and out. Thus, heat transfer between engine components and external heat source/sinks contribute to the external irreversibility of the engine, while viscous effects contribute to the internal irreversibility of the engine. Both external irreversibility and internal irreversibility lower the performance of the engine and cause loss in the available work.

CONCLUSIONS

The cycle of the resonant MEMS-based micro heat engine has been acquired experimentally and has been characterized using both pressure-volume and temperature-entropy diagrams. The working cycle is nearly rectangular in shape and consists of two constant temperature processes and two constant volume processes. The measured second law efficiency of the micro heat engine is 16%.

REFERENCES

1. Frechette, L., Lee, C., Arslan, S., and Liu, Y-C., 2003, "Design of a Microfabricated Rankine Cycle Steam Turbine for Power Generation," Paper No. IMECE2003-42082, Washington, D.C.
2. Fu, K., Knobloch, A. J., Marinez, F. C., Walther, D. C., Fernandez-Pello, C., Pisano, A. P., and Liepmann, D., 2001, "Design and Fabrication of a Silicon Based MEMS Rotary Engine," Paper No. IMECE2001/MEMS-23925, New York, NY.
3. Isomura, K., Murayama, M., Teramoto, S., Hikichi, K., Endo, Y., Togo, S., and Tanaka, S., 2006, "Experimental Verification of the Feasibility of a 100 W Class Micro-Scale Gas Turbine at an Impeller Diameter of 10mm," J. Micromech. Microeng., **16**, pp. S254- S261.
4. Nakajima, N., Ogawa, K., and Fujimasa, I., 1989, "Study on Micro Engines—Miniaturizing Stirling Engines for Actuators and Heat Pumps," IEEE Micro electro mechanical system Workshop, Salt Lake City.
5. Herrault, F., Crittenden, T., Yorish, S., Birdsell, E., Glezer, A., and Allen, M. G., 2008, "A Self-Resonant, MEMS-Fabricated, Air-Breathing Engine," Solid-State Sensors, Actuators, and Microsystems Workshop, Hilton Head Island, South Carolina.
6. Bardaweel, H.K., Anderson, M. J., Richards, R. F., and Richards, C. D., 2008, "Optimization of the Dynamic and Thermal Performance of a Resonant Micro Heat Engine," J. Micromech. Microeng. **18** (10), 104014.
7. Bardaweel, H., Anderson, M., Richards, R., and Richards, C., 2010, "Cyclic Operation of a MEMS-Based Resonant Micro Heat Engine: Experiment and Model," J. Appl. Phys., **107**, 104901.
8. Cho, J., Wiser, T., Richards, C., Bahr, D., and Richards, R., 2007, "Fabrication and Characterization of a Thermal Switch," Sensors and Actuators A: Physical, 133 (1), pp. 55-63.
9. Vlassak, J. J., and Nix, W. D., 1992, "A New Bulge Test Technique for the Determination of Young's Modulus and Poisson's Ratio of Thin Films," J Mater Res.,**7** (12), pp.3242–3249.